

The HeI₂ van der Waals complexes in a ‘free-rotor’ configuration

V V Baturo, S S Lukashov, S A Poretsky, A M Privilov  and A I Zhironkin

Department of Physics, Saint-Petersburg State University, SPbSU, 7/9 Universitetskaya nab., St. Petersburg, 199034, Russia

E-mail: a.privilov@spbu.ru

Received 26 July 2019, revised 1 November 2019

Accepted for publication 15 November 2019

Published 6 January 2020



CrossMark

Abstract

The HeI₂(E0_g⁺, $v_E = 0-6$, $n_E > 0$) van der Waals complexes in a free-rotor configuration populated in the excitation pathway via HeI₂(B0_u⁺, $v_B = 19$, $n_B = 2-4$) intermediate levels have been studied utilizing laser-induced luminescence spectroscopy methods. Analysis of the excitation pathway has been performed, and the I₂(E0_g⁺ → B0_u⁺, and D0_u⁺ → X0_g⁺) luminescence spectra have been measured. These I₂(E and D) molecules are the product of the HeI₂(E, $v_E = 0-6$, n_E) vibrational and electronic predissociation, respectively. We have defined the probabilities of the HeI₂(E, $v_E = 0-6$, n_E) predissociation channels, vibrational populations of the I₂(E and D) states as well as binding energies of the HeI₂(E, $v_E = 0-6$, n_E , $J = 0$) states. A modified *ab initio* potential of the HeI₂(E) state has been used to explain experimental results.

Supplementary material for this article is available [online](#)

Keywords: van der Waals complexes, iodine molecule, potential energy surface, ion-pair states

(Some figures may appear in colour only in the online journal)

1. Introduction

The van der Waals (vdW) complexes of diatomic halogens with rare gas atoms, due to their relative simplicity, have proved to be ideal model systems for fundamental investigations of molecular photofragmentation dynamics and intermolecular bonding (see [1–15] and references). Dissociation energies and frequencies of vdW modes have been determined for a wide range of vdW complexes, RgHal₂, in valence states, and their decay dynamics has been studied experimentally (see [1–3, 5, 6, 10, 14] and references). Detailed theoretical analysis of potential energy surfaces (PESs) of the complexes and their dynamical behavior has been carried out, also (see [1, 3, 4, 6–9, 11–13] and references).

High-level *ab initio* calculations of HeI₂(X0_g⁺, B0_u⁺ and E0_g⁺) complex PESs have been performed in [4, 7, 11, 12]. The HeI₂ *T*-shaped, linear as well as ‘free-rotor’ complexes, which vibrational wave functions are delocalized over $\theta = 0^\circ-360^\circ$, have been analyzed [6]. It has been shown in particular that:

- The degenerate X, $v_X = 0$, $n_X = 0, 1$ vdW levels ($E = -15.72$ cm⁻¹ relative to dissociation limit) are localized in the linear well, whereas $n_X = 2$ one ($E = -15.51$ cm⁻¹) is localized in the *T*-shaped well. The $n_X \geq 3$ levels ($E \geq -8.3$ cm⁻¹) have energies above the barrier between linear and *T*-shaped configurations and are spread over all θ values [9].
- The B, $v_B = 0$, $n_B = 0$ vdW level of the HeI₂ complex ($E = -12.33$ cm⁻¹) is localized in the *T*-shaped configuration, whereas $n_B = 1-6$ ($E = -8.36 - -2.34$ cm⁻¹) wave functions are spread over all θ values [7].
- The binding energy of the E, $v_E = 0$, $n_E = 0$ vdW level is $D_0^{E,0} = 16.85$ cm⁻¹, and this level is localized in the *T*-shaped configuration. The $n_E = 1$ level ($E = -10.68$ cm⁻¹ relative to the dissociation limit) is localized around $\theta = 70^\circ$ and 110° , and $n_E \geq 2$ levels ($E \geq -7.74$ cm⁻¹) show oscillatory character over all θ values [12].

Experimental studies on the HeI₂(E) have been performed for the first time in [6], and, recently, we have investigated the *T*-shaped HeI₂(E) vdW complex conformer [16, 17]. In general, the RgI₂(E) complex can dissociate with

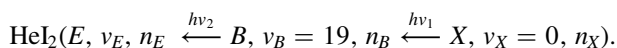
the formation of a Rg atom and I₂ in ion-pair (IP) states of the first tier, namely, $E0_g^+$, $D0_u^+$, $\beta 1_g$, $\gamma 1_u$, $D'2_g$ and $\delta 2_u$. For HeI₂, we have observed the luminescence of I₂(E) and I₂(D0_u⁺, D'/2_g) which are products of vibrational (VP) and electronic (EP) predissociation of the T-shaped HeI₂(E) complex, respectively. We have determined binding energies of the HeI₂(E, $\nu_E = 0-2$, $n_E = 0$) complexes, vibrational populations of the E, D states, and branching ratios (*b.r.*) of VP and EP channels.

This paper, devoted to spectroscopic characteristics and decay dynamics of HeI₂(E) vdW complexes in the free-rotor configuration, continues our studies on RgI₂(E) complexes, Rg = He, Ne, Ar, Kr [16–21]. Here, we have obtained and discussed product state distributions of the free-rotor HeI₂(E, $\nu_E = 0-6$, n_E) complex VP and EP as well as binding energies of this complex vibrational levels. We have assigned bands in excitation spectra assuming HeI₂(E ← B) transition follows the $\Delta n = n_E - n_B = 0$ selection rule. To calculate binding energies and Franck–Condon factors (FCFs) we have modified *ab initio* PES of Kalemos *et al* [12].

2. Experiment and analysis procedure

2.1. The OODR scheme

The procedure of preparation of HeI₂(E) complexes and detecting products of their VP and EP channels has been discussed in [16–21] (see [22, 23] and references, also). Briefly, HeI₂(X0_g⁺) vdW complexes were formed in a pulsed supersonic jet expansion (pulse width ~ 200 μ s). The gas mixture was prepared by passing He (backing pressure, $p_{\text{He}} = 40$ atm, typically) through a bubbler packed with a mixture of iodine crystals and polytetrafluoroethylene facing at 75 °C (iodine vapor pressure was ~ 10 Torr). Two counter-propagating temporally overlapped unfocused laser beams, crossing the molecular beam at 10 ± 1 mm downstream distance, were utilized to populate HeI₂(E) using a two-step two-color excitation scheme (figure 1)



The $h\nu_1$ and $h\nu_2$ laser pulses were generated from Quantel laser system consisting of two tunable dye TDL90 lasers pumped by YG981C Nd:YAG one. The $h\nu_1$ laser pulse energy in the chamber was ~ 3 mJ/pulse, and the $h\nu_2$ laser pulse energy was (0.1–0.4) mJ/pulse depending on λ_2 value. Dimensions of the $h\nu_1$ and $h\nu_2$ beams at ~ 10 mm downstream the nozzle pinhole were ~ 6 mm in diameter, and radiant exposures were $\sim 1 \times 10^6$ W cm⁻² and $\sim (0.04-0.16) \times 10^6$ W cm⁻², respectively.

It should be noted that the fundamental YG981C laser harmonic consists of 4 spectral components ν_f^i with the energy gap between neighboring lines ~ 1.6 cm⁻¹ [16, 17]. Because of that, the $h\nu_2$ laser radiation, produced by mixing of the fundamental Nd:YAG laser harmonics and the TDL laser fundamental output in KDP crystal, also consists of 4 spectral components. The $h\nu_1$ laser pulse is generated directly in one of the TDL90 laser. The λ_1 and λ_2 wavelengths were

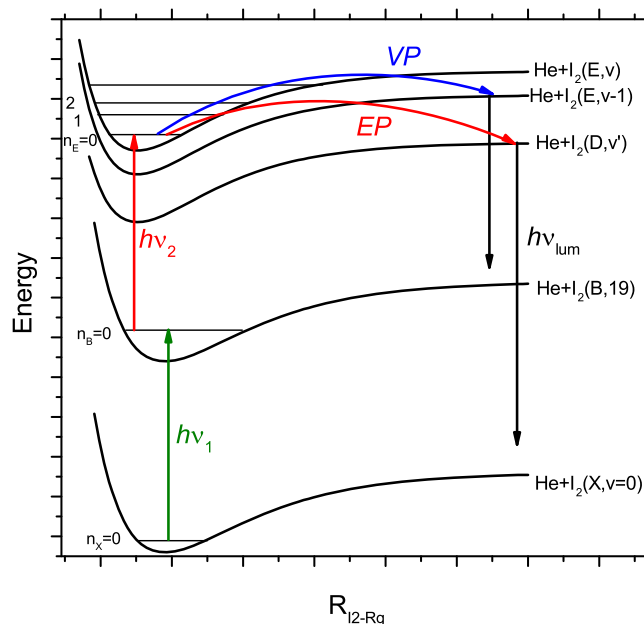


Figure 1. Schematic diagram describing excitation as well as VP and EP of the HeI₂(E) complex.

measured by means of WS6 wavelength meter (Ångstrom) with ± 0.01 Å uncertainty.

Dispersed luminescence spectra were recorded using monochromator MDR2/photomultiplier tube (PMT) FEU100 system with spectral resolution FWHM ≥ 5 Å. Besides, integrated luminescence of the HeI₂(E) complex decay products in the $\lambda_{\text{lum}} \approx 2600-3800$ Å spectral range was simultaneously recorded using PMT FEU71/glass filter UFS2 system. It was used to correct the dispersed luminescence signal on integral luminescence intensity change caused in particular by $h\nu_1$ and $h\nu_2$ laser pulse energy changes. Excitation spectra of I₂(IP) state luminescence (scan of λ_2 at selected λ_1 , λ_{lum} wavelengths) and action spectra (scan of λ_1 at selected λ_2 , λ_{lum} wavelengths) were measured and analyzed to understand the mechanism of the optical population of the luminescent species. Excitation and action spectra for integrated luminescence, $\lambda_{\text{lum}} \approx 2600-3800$ Å, were measured as well.

The procedures of simulation of luminescence spectra have been described in detail elsewhere (see [24–26] and references). The HeI₂(E, ν_E , n_E) can decay to He + I₂(E) (VP) and He + I₂(other IP states) (EP). Vibrational state distributions of the complex predissociation products were obtained after luminescence spectra simulation. Briefly, a sum of calculated spectra of luminescence of a several vibronic levels of iodine molecule IP states, I₂(IP, ν_{IP}), IP = $E0_g^+$, $D0_u^+$, (contributions of the vibronic levels were used as adjustable parameters) was fit to the experimental spectra, corrected by the changes of integrated luminescence and a spectral sensitivity function of the condenser/monochromator/detector system (see [24–26] and references for details).

Excitation bands corresponding to 4 components of $h\nu_2$ laser radiation are saturated (see [16, 17] and references). Therefore, to simplify excitation and action spectra and

eliminate two-photon transitions in I_2 molecules and HeI_2 complexes (see section 3), they were measured with $h\nu_2$ radiation intensities decreased ~ 60 times by neutral NS10 filter. Two bands of excitation spectra corresponding to the $\nu_f^1 = 9395.12 \pm 0.02 \text{ cm}^{-1}$ and $\nu_f^2 = 9393.53 \pm 0.07 \text{ cm}^{-1}$ strongest components were observed in these cases (see figure SD1 is available online at stacks.iop.org/JPB/53/035101/mmedia and section 3).

2.2. Computational methods

We have used Jacobi coordinates r , R , θ for calculations; r is the I–I internuclear distance, R is the distance between He atom and I_2 center of mass, and θ is the angle between the r and R vectors. The Hamiltonian in this coordinate system is as follows:

$$\hat{H} = -\frac{\hbar^2}{2\mu_r} \frac{\partial^2}{\partial r^2} - \frac{\hbar^2}{2\mu_R} \frac{\partial^2}{\partial R^2} + \frac{\hat{j}^2}{2\mu_r r^2} + \frac{\hat{l}^2}{2\mu_R R^2} + V(r, R, \theta). \quad (1)$$

Here μ_r and μ_R are the reduced masses associated with r and R , respectively, $1/\mu_r = 2/m_I$, $1/\mu_R = 1/m_{He} + 1/2m_I$, \hat{j} and \hat{l} are the angular momentum operators corresponding to the r and R vectors. The r value has been kept frozen at the equilibrium I–I distances, $r_e = 2.666 \text{ \AA}$, 3.024 \AA and 3.593 \AA for the X , B and E states, respectively. The PESs, $V(r_e, R, \theta)$, have been constructed using *ab initio* data from [9] (X state), [7] (B state), [12] (E state). It is known that the X and B surfaces describe experimental excitation spectra of the $I_2(B)$ luminescence adequately [6]. All calculations have been performed for the nonrotating complex with the total angular momentum operator $\hat{J} = \hat{j} + \hat{l} = 0$. The time-independent two-dimensional Schrödinger equation has been solved using WavePacket utility [27] with the discrete variable representation (DVR) for R and θ coordinates. A grid of 100 equally spaced points on R and 51 DVR points associated with Legendre polynomials $P_k(\cos \theta)$ have been used. Analysis of the first 7 vibrational levels of the vdW mode has been performed. Potential wells of the $HeI_2(X, B$ and $E)$ states are shallow, and it is not correct to describe vdW vibrational states in terms of stretch and bend modes. The only one n quantum number represents them. Once the energies and wave functions have been evaluated, FCFs of $HeI_2(E - B$ and $B - X)$ transitions have been calculated to compare them with the experimental data.

3. Results

The excitation spectrum of luminescence recorded in the $I_2(B, 19 - X, 0)$ and $HeI_2(B, 19 - X, 0)$ transition spectral region is given in figure 2. The spectrum contains two discrete bands at 17801.4 cm^{-1} and 17804.9 cm^{-1} associated with the free I_2 molecule and HeI_2 complex in the T -shaped configuration, respectively, and a wide band (full-width half-maximum, $\text{FWHM} \approx 4 \text{ cm}^{-1}$) at $\nu_{max} = 17811 \text{ cm}^{-1}$.

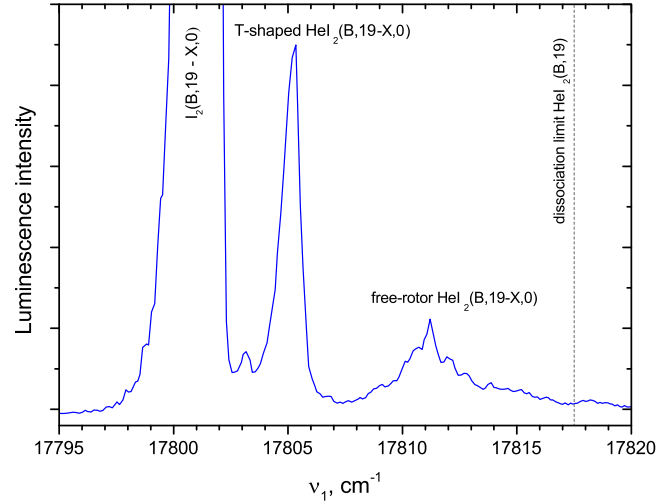


Figure 2. Excitation spectrum of luminescence of the $I_2(B, 19)$ and the $HeI_2(B, 19)$ complex VP products. The PMT FEU100 + KS10 glass filter, $\lambda > 600 \text{ nm}$, was used. Positions of the bands corresponding to the transition to the T -shaped and free-rotor $HeI_2(B, 19)$ complexes are shown. The dashed line marks the dissociation limit of the $HeI_2(B, 19)$ complex.

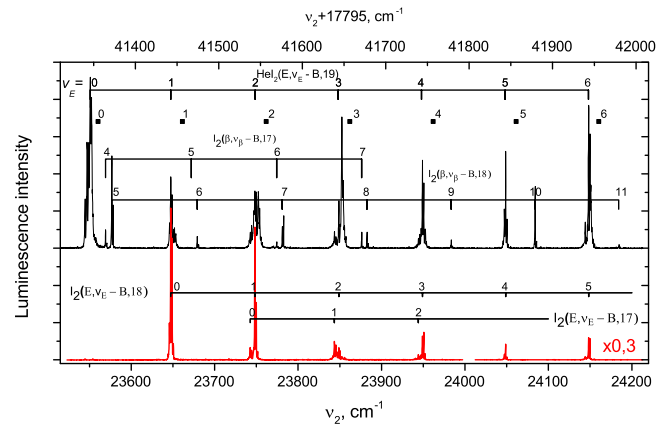


Figure 3. Excitation spectra of luminescence in the $E \rightarrow B$, $\lambda_{lum} \approx 4284 \text{ \AA}$, (red (gray) line) and UV spectral range, $\lambda_{lum} \approx 2600\text{--}3800 \text{ \AA}$ (black line) measured at $\lambda_1 = 5614.47 \text{ \AA}$ ($\nu_1 = 17811.1 \text{ cm}^{-1}$, free-rotor $HeI_2(B, 19, n_B \approx 3 \leftarrow X, 0, n_X = 0, 1)$ transition). Energy of transitions to the $I_2(E, \nu_E = 0\text{--}6, J_E = 0)$ states corresponding to the most intense spectral $\nu_f^1 = 9395.12 \text{ cm}^{-1}$ component (dissociation limits of the $HeI_2(E, \nu_E = 0\text{--}6, n_E)$ complexes, see section 2) are marked out as black squares. The bands corresponding to the $I_2(E, \nu_E = 0\text{--}5 \leftarrow B, \nu_B = 17, 18$ and $\beta_{1g}, \nu_\beta = 5\text{--}7 \leftarrow B, \nu_B = 17, 18)$ transitions are shown. Groups of excitation bands of the $I_2(IP \rightarrow \text{valence states})$ luminescence corresponding to the $HeI_2(E, \nu_E = 0\text{--}6, n_E)$ states are marked out as $\nu_E = 0\text{--}6$.

According to [6], this wide band is ascribed to the linear complex $HeI_2(B, 19, n_B = 1\text{--}6 \leftarrow X, 0, n_X = 0, 1)$ transitions, though, according to [7], the $n_B = 1\text{--}6$ ($E = -8.36\text{--}-2.34 \text{ cm}^{-1}$ relative to dissociation limit) wave functions are spread over all θ values.

Survey excitation spectra of luminescence in visible, $\lambda_{lum} \approx 4284 \text{ \AA}$, and UV spectral ranges, $\lambda_{lum} \approx 2600\text{--}3800 \text{ \AA}$ measured at $\lambda_1 = 5614.47 \text{ \AA}$ ($\nu_1 = 17811.1 \text{ cm}^{-1}$,

Table 1. Branching ratios, *b.r.*, of the $\text{HeI}_2(E, v_E, n_E)$ VP and EP product formation and maximal vibronic state determined by simulation of the $\text{I}_2(E \rightarrow B \text{ and } D \rightarrow X)$ luminescence spectra measured at the $\text{HeI}_2(E, v_E, n_E = 0 \leftarrow B, 19, n_B)$ bands ($v_{\text{IP}}^{\text{max}}$).

v_E	$v_D^{\text{max}}/b.r.$	$v_E^{\text{max}}/b.r.$
0	4/0.97	—
2	6/0.33	1/0.67
3	7/0.27	2/0.73
6	10/0.21	5/0.77

$\text{HeI}_2(B, 19, n_B \approx 3 \leftarrow X, 0, n_X = 0, 1)$ transition, see figure 3 and below) are plotted in figure 3.

Seven groups of the excitation bands located lower than the dissociation limits of the $\text{HeI}_2(E, v_E = 0-6, n_E)$ complexes are called $v_E = 0, 1$ and so on groups in figure 3. They consist of the bands corresponding to the $\text{HeI}_2(E, v_E, n_E \leftarrow B, 19, n_B)$ transitions ($v_E = 0-6$), as well as $E, v_E \leftarrow B, v_B$ transitions in a free (isolated) iodine molecule. The $\text{HeI}_2(E, v_E = 0, n_E \leftarrow B, 19, n_B)$ band has been assigned thus: this is the band in figure 3 with the least wavenumber; all bands with $\nu_2 < 23\,550\text{ cm}^{-1}$ may only be assigned to $\text{I}_2(\beta 1_g, v_\beta \leftarrow B, v_B)$ transitions in a free I_2 molecule (figure SD2).

According to the literature data [6, 9], the binding energy of the linear $\text{HeI}_2(X, 0, n_X = 0, 1)$ complex is $D_0^X \approx 16\text{ cm}^{-1}$. The $\text{HeI}_2(E)$ complex term energy (upper *x*-axis in figure 3) relative to that of the $\text{I}_2(X, v_X = 0, J_X = 0)$ is $\nu_1 + \nu_2 - D_0^X$. The binding energies of the $\text{HeI}_2(E, v_E = 0-6, n_E)$ complexes can be determined as the energy gaps, ΔE , between $(17\,795 + \nu_2)$ of the transitions corresponding to the $\nu_f^1 = 9395.12\text{ cm}^{-1}$ component (see caption to figure 3) and energy of transitions to the $\text{I}_2(E, v_E = 0-6, J_E = 0)$ states.

Probabilities of the decay channels (EP and VP) branching ratios, *b.r.*, have been estimated as the ratios of integrated partial intensity of the selected IP state luminescence to the sum of all integrated intensities (see table 1). Luminescence spectra, measured at the $\text{HeI}_2(E, v_E \leftarrow B, 19)$ transition bands, show that $\text{I}_2(D \rightarrow X, E \rightarrow B)$ and very weak luminescence, $\lambda_{\text{lum}} \approx 342\text{ nm}$, *b.r.* ≈ 0.03 and 0.02 at $v_E = 0$ and 6 bands, respectively, occurs (see figures 4, 5 as examples and figures SD3, 4, also). The $\text{HeI}_2(E, v_E, n_E) \rightarrow \text{He} + \text{I}_2(E, v_E - \Delta v_E)$, $\Delta v_E = 0$, VP channels are energetically closed, as it occurs for the *T*-shaped $\text{HeI}_2(E, v_E, n_E)$ complexes (see [16, 19–21] and references). A weak luminescence, *b.r.* ≈ 0.1 , occurs in the $\lambda_{\text{lum}} = 4000-4400\text{ \AA}$ spectral range at the $\Delta v_E = 0$ band. This luminescence belongs to the $\text{HeI}_2(E, v_E = 0, n_E)$ complex itself.

Excitation spectra measured at the $v_E = 0$ group and corresponding action spectra are given in figures 6, 7.

One sees in figure 6 the only group of bands (*A, B, C*) in the excitation spectra. Due to the complex spectral structure of the Nd:YAG laser generation in our experiments, they are split into two groups corresponding to the ν_f^1 and ν_f^2 strong components (see section 2). Similar features have been observed at the $v_E = 1-6$ groups. Below, we will consider left band, corresponding to the ν_f^1 component. FWHM of the

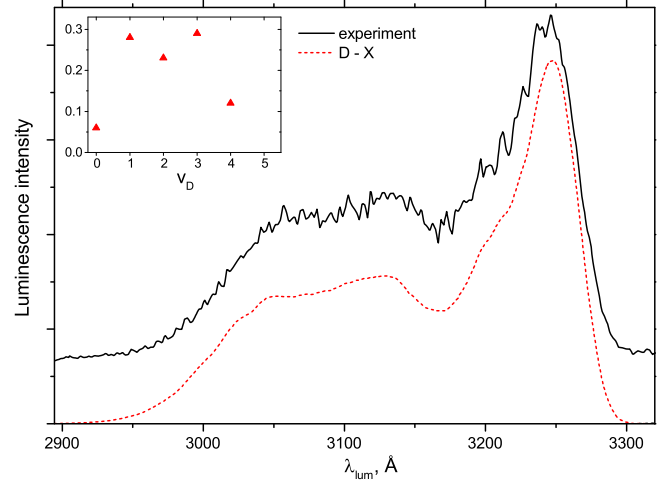


Figure 4. Experimental (solid line) and simulated (dashed line) luminescence spectra in the $\lambda_{\text{lum}} = 2900-3550\text{ \AA}$ spectral range at the $v_E = 0$ group of bands, $\nu_2 = 23\,550.9\text{ cm}^{-1}$. Spectral resolution FWHM = 20 \AA . The experimental spectrum is offset for clarity. Populations of the *D*, v_D vibronic levels are given in the inset.

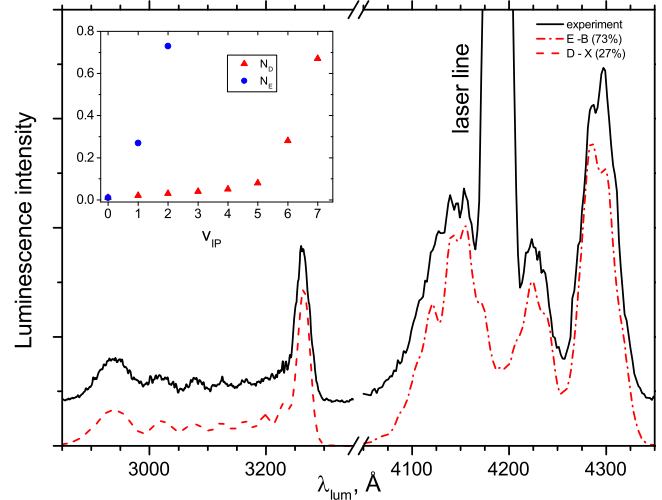


Figure 5. Experimental (solid line) and simulated (dashed lines) luminescence spectra in the $\lambda_{\text{lum}} = 2800-4400\text{ \AA}$ spectral range at the $v_E = 3$ group of bands, $\nu_2 = 23\,852.4\text{ cm}^{-1}$ spectral resolution FWHM = 20 \AA . The experimental spectrum is offset for clarity. Populations of the *D*, v_D and *E*, v_E vibronic levels are given in the inset. The λ_2 laser line is marked.

subbands is $\sim 0.35\text{ cm}^{-1}$, and energy gaps between them are ($\sim 0.4-0.6\text{ cm}^{-1}$), significantly lower than between corresponding to neighboring n_E levels (see table 4 in [12]). To assign these subbands to the n_B vdW modes, we measured action spectra at them. The action spectrum bands are marked out as corresponding to $n_B = 2, 3, 4$ in figure 7 (see section 4). The *B* subband, $\nu_2 = 23\,552.1\text{ cm}^{-1}$, has higher relative intensity compared to those of the *A, C* subbands than the *B* subband, $\nu_2 = 23\,550.49\text{ cm}^{-1}$ since transition in the former is overlapped with the $\text{I}_2(\beta, v_\beta = 10, J_\beta \approx 10 \leftarrow B, 24, J_B \leftarrow X, 2, J_X)$ one.

The *A* subband near $23\,550\text{ cm}^{-1}$ measured at $\nu_1 = 17\,811.1\text{ cm}^{-1}$ is overlapped with *B* and *C* bands.

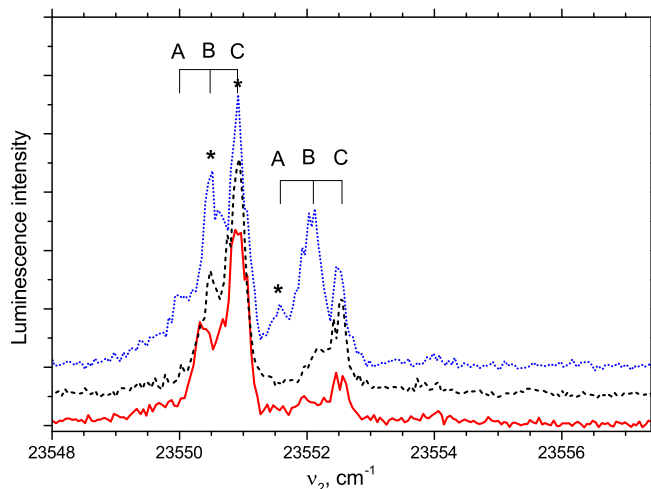


Figure 6. Excitation spectra of luminescence in the $\nu_2 = 23\,540\text{--}23\,560\text{ cm}^{-1}$ (the $\nu_E = 0$ group) corresponding to the UV spectral range, $\lambda_{\text{lum}} \approx 2600\text{--}3800\text{ \AA}$ measured at $n_B = 4$ band (red, solid line), $n_B = 3$ band (blue, dotted line) and $n_B = 2$ band (black, dashed line), see figure 7. The bands for which action spectra have been measured are marked out by asterisks.

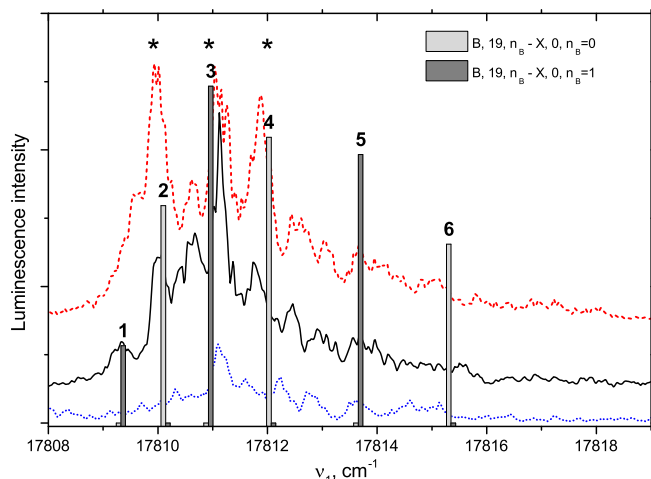


Figure 7. Action spectra for UV luminescence measured at $\nu_E = 0$ group of bands for A, B and C subbands, $\nu_2 = 23\,551.5$ (blue, dotted line), $23\,550.5$ (black, solid line) and $23\,550.9$ (red, dashed line), respectively, see figure 6. The bands, $n_B = 2, 3, 4$, for which excitation spectra have been measured are marked out by stars. FCFs of the $\text{HeI}_2(B, 19, n_B - X, 0, n_X = 0, 1)$ and $B, 19, n_B = 0 - X, 0, n_X = 2)$ transitions as well as the assignment of n_B are presented as bars (see section 4). Energies of these transitions are corrected by the difference between calculated and experimental D_0^X values (see [9]).

Therefore, we measured action spectra for the A subband near $23\,551.5\text{ cm}^{-1}$.

Excitation spectrum of the $\text{HeI}_2(B, 19)$ complex VP product luminescence (see figure 3) shows the $\text{HeI}_2(B, 19, n_B)$ levels populated in the $\text{HeI}_2(B, 19, n_B \leftarrow X, 0, n_X)$ transitions, whereas action spectra (figure 7) show $\text{HeI}_2(B, 19, n_B)$ levels from which $\text{HeI}_2(E, \nu_E, n_E \leftarrow B, 19, n_B)$ transitions occur. It has been shown in [6, 7] that the $\text{HeI}_2(B, 19, n_B = 2\text{--}5 \leftarrow X, 0, n_X = 0, 1)$ transitions are the strongest in the free-rotor conformer (see section 4).

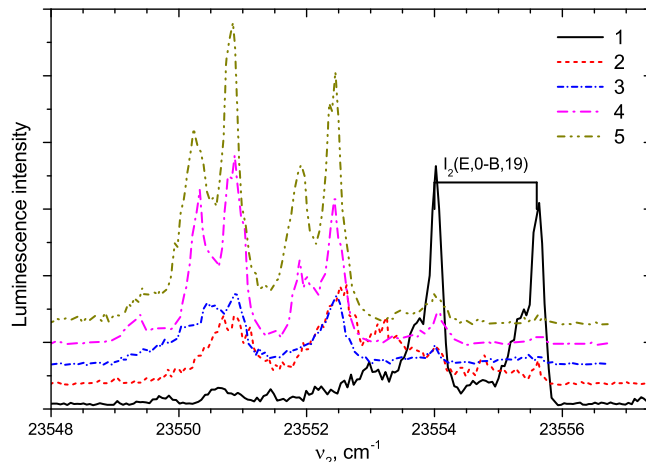


Figure 8. Excitation spectra of the UV luminescence in the $\nu_2 = 23\,548\text{--}23\,560\text{ cm}^{-1}$ (the $\nu_E = 0$ group) corresponding to the UV spectral range, $\lambda_{\text{lum}} \approx 2600\text{--}3800\text{ \AA}$ measured at $\nu_1 = 17\,819.0$ (1), $17\,817.4$ (2), $17\,815.8$ (3), $17\,814.2$ (4), $17\,812.6\text{ cm}^{-1}$ (5).

Excitation spectra given in figure 6 are measured in the ν_1 range corresponding to $\text{HeI}_2(B, 19, n_B = 2\text{--}4 \leftarrow X, 0, n_X = 0, 1)$ transitions. To check if the n_E vdW level can be populated from $n_B > 4$ levels we measured excitation spectra in wider ν_1 range, up to dissociation limit of the $\text{HeI}_2(B, 19)$ complex ($\nu_1 = 17\,817.5\text{ cm}^{-1}$ [7]) and higher (figure 8).

Spectrum (1) in figure 8 measured at $\nu_1 = 17\,819.0\text{ cm}^{-1}$ corresponds to a *bound-free* $B \leftarrow X$ transition in the complex with subsequent dissociation to the $\text{I}_2(B, 19) + \text{He}$. Another (2)–(5) spectra are broad and correspond to the *bound-bound* $B \leftarrow X$ transition in the complex (see figure 2 and [6]). The bands in the $\nu_2 = 23\,549\text{--}23\,553\text{ cm}^{-1}$ range become more and more distinct with ν_1 decreasing, and at $\nu_1 = 17\,814.2, 17\,812.6\text{ cm}^{-1}$, they are similar to the A, B, C subbands presented in figure 6 and measured in the $\nu_1 < 17\,812\text{ cm}^{-1}$ spectral range

One sees that the population of the free-rotor $\text{HeI}_2(E)$ complex occurs in rather narrow $\nu_2 \approx 23\,550\text{--}23\,551.5\text{ cm}^{-1}$ range. The C subband occurs in excitation spectra measured at all the ν_1 wavenumbers used (figures 6, 8), and the A band corresponds to the lowest $\text{HeI}_2(E, \nu_E = 0, n_E)$ levels observed.

One should note that excitation spectra given in figures 6, 8 differ significantly from those given in figure 5 of [6]: we have not observed the bands corresponding to total excitation energy $\sim 41\,455.7$ and $41\,458.4\text{ cm}^{-1}$ (the $\text{HeI}_2(E, 1, n_E = 0, 1 \leftarrow B, 23, n_B = 3)$ transitions in [6]). We have shown in [16, 19] that the $41\,455.7\text{ cm}^{-1}$ band corresponds to two-photon $\text{I}_2(E, 1 \leftarrow X, 0)$ transition ($41\,456.33\text{ cm}^{-1}$ for $J_E = 1, J_X = 0$). The $41\,458.4\text{ cm}^{-1}$ band corresponds to two-photon $\text{HeI}_2(E, 1, n_E = 0 \leftarrow X, 0, n_X = 0, 1)$ transition (binding energies of the $n_X = 0, 1$ and $n_E = 0$ states is 15.72 cm^{-1} [9] (theory) and 14 cm^{-1} [16] (experiment), respectively). We did not see these transitions, since the $h\nu_2$ radiation intensities were heavily reduced (see section 2).

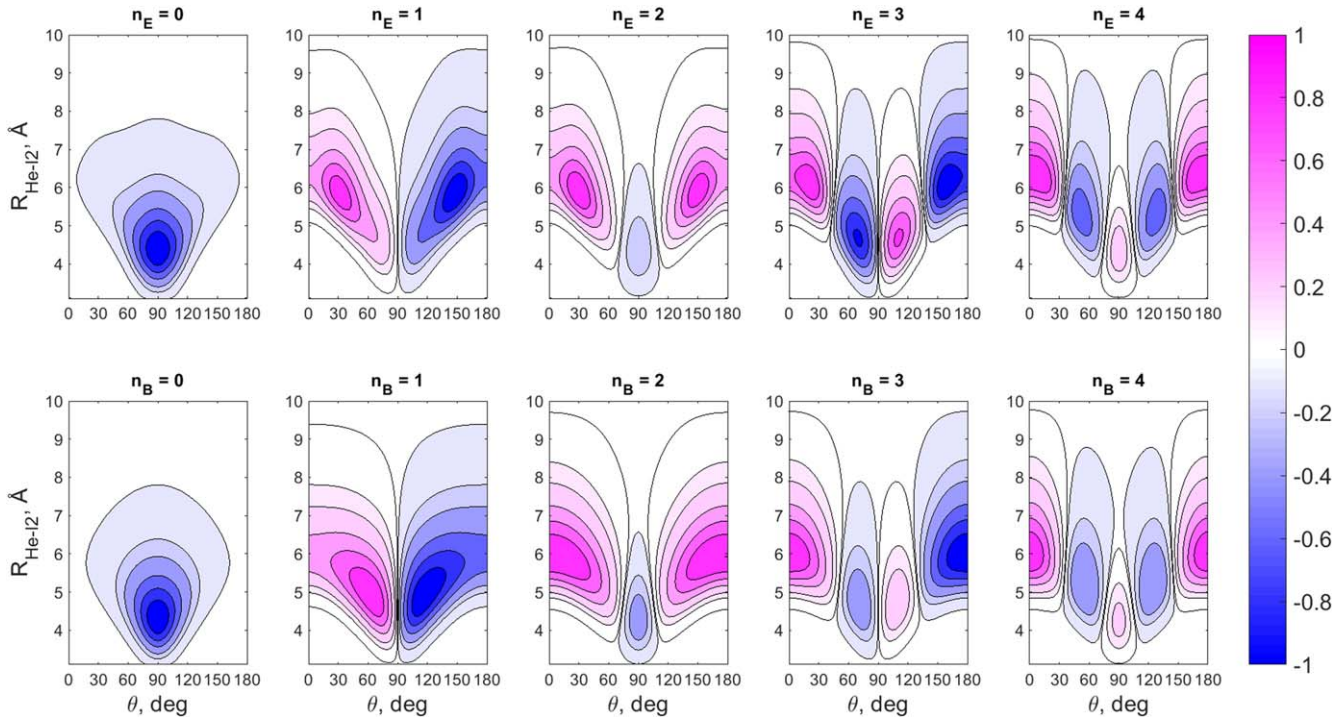


Figure 9. Contour plots of the vdW vibrational mode wave functions for the $\text{HeI}_2(B$ and E) states in Jacobi coordinates.

4. Discussion

According to [11], the only vibrational level of the X state, $n_X = 2$, is localized in the T -shaped configuration, two degenerated $n_X = 0, 1$ levels are at the linear geometry, while other state, $n_X > 2$, wave functions are spread over the whole range of θ values but located mainly near-linear configuration. As to the B state, there is also the only level, $n_B = 0$, of the T -shaped configuration [7], while other states, $n_B > 0$, are delocalized. So, the only B , $n_B = 0 \leftarrow X$, $n_X = 2$ transition for the T -shaped conformer is observable in the excitation spectra [6, 16].

Contour plots of the vdW vibrational mode wave functions for the $\text{HeI}_2(B$ and E) calculated as it is described in section 2.2 are given in figure 9. One sees in this figure that symmetry of the wave function of both, B and E , states to permutation of the nuclei are different for even and odd n : they are even for even n , and odd for odd n . Therefore the $\text{HeI}_2(E, \nu_E, n_E \leftarrow B, \nu_B, n_B)$ transitions follow the $\Delta n = \text{even}$ selection rule.

The n_B levels of different parity can be populated from the $n_X = 0, 1$ ground state levels. These $\text{HeI}_2(B, 19, n_B \geq 1 \leftarrow X, 0, n_X = 0, 1)$ transitions make a major contribution to the wide band in 17 808–17 815 cm^{-1} spectral range in figure 2. In addition, $\text{HeI}_2(B, \nu_B, n_B \leftarrow X, 0, n_X = 0, 1)$ bands must have a wide, up to 1 cm^{-1} , rotational structure [6] that also defines this band shape. However, action spectra (figure 7) are purer. It means that a few numbers of n_B levels are involved in the $\text{HeI}_2(E \leftarrow B \leftarrow X)$ two-step transitions in the complex. One sees in figure 7, that the action spectrum contains three subbands, and the population of the E state

occurs via the $\text{HeI}_2(B, 19, n_B = 2, 3, \text{ and } 4)$ intermediate states.

All the $\text{HeI}_2(E \leftarrow B)$ excitation spectra corresponding to the $n_B = 2, 3$ and 4 intermediate states are slightly different but located in the same range of ν_2 (figure 6). This feature can be explained, supposing that it can be ascribed to $\Delta n = 0$ sequences. Indeed, PESs of the B and E states are similar; they have the only global minima at T -shaped configuration [7, 12]. The $\text{HeI}_2(E, \nu_E, n_E > 0)$ vibrational wave functions are delocalized and are spreading over all angle values just as those of the B state, so the $\text{HeI}_2(E \leftarrow B, \Delta n = 0)$, transitions are most probable.

However, binding energies of the $\text{HeI}_2(E)$ state vdW levels calculated using $\text{HeI}_2(E)$ PES from [12] are not consistent with our experimental results (see table 2). To reproduce the data of this work and [16, 19] we have corrected *ab initio* potential from [12] multiplying it by

$$\sigma(\theta) = (1 + \beta_1 \sin^2 \theta)(1 + \beta_2 \cos^2 \theta). \quad (2)$$

Such function allows us to correct T -shaped and linear configuration well depths almost independently. The best agreement with the experiment has been reached by modifying the potential from [12] with $\beta_1 = -0.15$ and $\beta_2 = +0.67$. Binding energies calculated using this modified potential compared with those from [12] are given in table 2.

One sees from table 2 that the $n = 2-4$ levels of both B and E states are almost equidistant. Therefore, the wavenumbers of the $\Delta n = 0$ sequence (2-2, 3-3, and 4-4) are close to each other and correspond to A, B and C subbands, respectively. However, calculated FCFs of $\Delta n = 2, 4$ sequences are also found to be non-zero which contradicts our experimental data (there are no additional bands in figure 7). To explain this feature, one has to modify PESs more substantially.

Table 2. Experimental and calculated binding energies of the $\text{HeI}_2(E, 0, n_E$ and B, ν_B, n_B) vdW levels.

n	B state		E state		
	[6]	[7]	This work (exp.)	[12]	This work (calc.)
0	12.8	12.3	14.1 [16, 19]	16.8	13.9
1	—	8.4		14.1	10.9
2	7.9	7.6	10.8 (A)		10.7
3	6.8	6.8	9.8 (B)		9.3
4	5.7	5.6	8.3 (C)		7.7

Comparison of the data on the maximal vibronic levels of the $I_2(E$ and $D)$ states populated and *b.r.* values (see table 1) with those obtained for the T-shaped $\text{HeI}_2(E, \nu_E, n_E)$ conformer [16, 19] shows the following:

- The $I_2(D, \nu_D = 3)$ vibronic level is populated in the T-shaped conformer whereas $I_2(D, \nu_D = 4)$ in the free-rotor configuration since the $\text{HeI}_2(E, \nu_E, n_E = 0)$ levels (binding energy $\sim 14 \text{ cm}^{-1}$ [16, 19]) are populated in the former, and the $\text{HeI}_2(E, \nu_E, n_E = 2-4)$ (binding energy $8.3-10.8 \text{ cm}^{-1}$ [16, 19]) in the latter. The $I_2(D, \nu_D = 4)$ level cannot be populated from the $\text{HeI}_2(E, \nu_E, n_E = 0)$ one since the former lies 3.4 cm^{-1} higher than the latter, but can be populated from the $\text{HeI}_2(E, \nu_E, n_E = 2-4)$ levels;
- The VP and EP probabilities differ significantly for the T-shaped and free-rotor conformers for the $\text{HeI}_2(E, \nu_E = 1, 2, n_E)$ levels. The EP probability is ~ 1.8 times higher than that of VP in the former [16, 19], whereas it ~ 2 times less for the latter, probably due to different locations of the $\text{HeI}_2(E, \nu_E, n_E)$ wavefunctions in these cases.

Finally, let us consider the experimental results presented in figure 8. One sees that each of excitation spectra (2)–(5) contains the band at $23\,549-23\,553 \text{ cm}^{-1}$ irrespective of the ν_1 value. This feature can be explained if one assumes the $\text{HeI}_2(B, 19, n_B \geq 1 \leftarrow X, 0, n_X = 0, 1)$ bands are broad. According to experimental data obtained in this work and in [6], the $\text{HeI}_2(B, \nu_B, n_B = 2-4 \leftarrow X, 0, n_X = 0, 1)$ bands are strongly overlapped, and transitions via all these n_B levels have to contribute to the two-step spectra. The $\text{HeI}_2(E, \nu_E, n_E) \leftarrow B, 19, n_B$ excitation band, in turn, have a narrow rotational structure since the PESs of the B and E states are similar, and transitions from different rotational levels J_B have similar frequencies. A simple rigid rotor model at the linear configuration of the HeI_2 complex gives that the $\text{HeI}_2(E \leftarrow B)$ transition band is two times narrower than that of the $\text{HeI}_2(B \leftarrow X)$ one. However, a comparison of the theoretical and experimental data obtained does not allow us to make certain statements.

5. Conclusion

In the $\text{HeI}_2(E, \nu_E = 0-6, n_E)$ free-rotor conformer, the two-step optical population is realized as follows: $\text{HeI}_2(E, \nu_E, n_E = 2-4 \xleftarrow{h\nu_2} B, \nu_B, n_B = 2-4 \xleftarrow{h\nu_1} X, 0, n_X = 0, 1)$ with

$\Delta n_B - n_X = |n_B - n_X| = \text{even progressions}$ and $\Delta n_E - B = |n_E - n_B| = 0$ sequences. The principal channel of the $\text{HeI}_2(E, \nu_E = 0-6, n_E)$ decay is vibrational predissociation (if it is energetically allowed). The probability of the complex electronic predissociation is *appr.* 2-3 times lower.

Acknowledgments

The authors acknowledge the Russian foundation for basic researches for grant 19-03-00148a and Saint-Petersburg State University Research park for the manufacture of experimental set-up elements in the framework of project 8459 # 123-8459.

ORCID iDs

A M Pravilov  <https://orcid.org/0000-0001-9880-5576>

References

- [1] Rohrbacher A, Halberstadt N and Janda K C 2000 *Ann. Rev. Phys. Chem.* **51** 405
- [2] Burroughs A and Heaven M C 2001 *J. Chem. Phys.* **114** 7027
- [3] Buchachenko A A, Halberstadt N, Lepetit B and Roncero O 2003 *Int. Rev. Phys. Chem.* **22** 153
- [4] Prosmi R, Valdés Á, Villarreal P and Delgado-Barrio G 2004 *J. Phys. Chem. A* **108** 6065
- [5] Darr J P, Glennon J J and Loomis R A 2005 *J. Chem. Phys.* **122** 131101
- [6] Ray S E, McCoy A B, Glennon J J, Darr J P, Lancaster J R and Loomis R A 2006 *J. Chem. Phys.* **125** 164314
- [7] Valdés Á, Prosmi R, Villarreal P, Delgado-Barrio G and Werner H-J 2007 *J. Chem. Phys.* **126** 204301
- [8] Valdés Á, Prosmi R, Villarreal P, Delgado-Barrio G, Lemoin G and Lepetit B 2007 *J. Chem. Phys.* **126** 244314
- [9] García-Gutierrez L, Delgado-Tellez L, Valdés Á, Prosmi R, Villarreal P and Delgado-Barrio G 2009 *J. Phys. Chem. A* **113** 5754
- [10] Zhang Y, Vidma K, Parker D H and Loomis R A 2009 *J. Chem. Phys.* **130** 104302
- [11] Delgado-Tellez L, Valdés Á, Prosmi R, Villarreal P and Delgado-Barrio G 2012 *Int. J. Quant. Chem.* **112** 2971
- [12] Kalmos A, Valdés Á and Prosmi R 2012 *J. Chem. Phys.* **137** 034303
- [13] García-Vela A 2014 *J. Phys. Chem. A* **118** 6395
- [14] Makarem C and Loomis R A 2016 *Chem. Phys. Lett.* **651** 119
- [15] Smalley R E, Levy D H and Wharton L 1976 *J. Chem. Phys.* **64** 3266
- [16] Baturo V V, Lukashov S S, Poretsky S A, Pravilov A M and Zhironkin A I 2016 *Chem. Phys. Lett.* **662** 250
- [17] Baturo V V, Lukashov S S, Poretsky S A and Pravilov A M 2017 *Eur. Phys. J. D* **71** 227
- [18] Baturo V V, Cherepanov I N, Lukashov S S, Poretsky S A and Pravilov A M 2016 *Chem. Phys. Lett.* **647** 161
- [19] Baturo V V, Kevorkyants R, Lukashov S S, Poretsky S A, Pravilov A M and Zhironkin A I 2016 *Chem. Phys. Lett.* **684** 357
- [20] Baturo V V, Lukashov S S, Poretsky S A and Pravilov A M 2018 *Chem. Phys. Lett.* **696** 26
- [21] Baturo V V, Lukashov S S, Poretsky S A and Pravilov A M 2019 *J. Phys. B: At. Mol. Opt. Phys.* **52** 145101

- [22] Akopyan M E, Baturo V V, Lukashov S S, Poretsky S A and Pravilov A M 2015 *Chem. Phys.* **462** 3
- [23] Akopyan M E, Baturo V V, Lukashov S S, Poretsky S A and Pravilov A M 2013 *J. Phys. B: At. Mol. Opt. Phys.* **46** 055101
- [24] Pravilov A M 2011 *Radiometry in Modern Scientific Experiments* (New York: Springer)
- [25] Akopyan M E, Baturo V V, Lukashov S S, Poretsky S A and Pravilov A M 2011 *J. Phys. B: At. Mol. Opt. Phys.* **44** 205101
- [26] Akopyan M E, Baturo V V, Lukashov S S, Poretsky S A and Pravilov A M 2012 *J. Chem. Phys.* **136** 234302
- [27] Schmidt B and Lorenz U 2017 *Comput. Phys. Commun.* **213** 223